

Microfluidic free interface diffusion: measurement of diffusion coefficients and evidence of interfacial-driven transport phenomena

Hoang-Thanh Nguyen, Anne Bouchaudy, and Jean-Baptiste Salmon
 CNRS, Solvay, LOF, UMR 5258, Univ. Bordeaux, F-33600 Pessac, France

(*Electronic mail: jean-baptiste.salmon-exterieur@solvay.com)

(Dated: 23 August 2022)

We have developed a microfluidic tool to measure the diffusion coefficient D of solutes in an aqueous solution, by following the temporal relaxation of an initially steep concentration gradient in a microchannel. Our chip exploits multilayer soft lithography and the opening of a pneumatic microvalve to trigger the interdiffusion of pure water and the solution initially separated in the channel by the valve, the so-called free interface diffusion technique. Another microvalve at a distance from the diffusion zone closes the channel and thus suppresses convection. Using this chip, we have measured diffusion coefficients of solutes in water with a broad size range, from small molecules to polymers and colloids, with values in the range $D \in [10^{-13} - 10^{-9}] \text{ m}^2/\text{s}$. The same experiments but with added colloidal tracers also revealed diffusio-phoresis and diffusio-osmosis phenomena due to the presence of the solute concentration gradient. We nevertheless show that these interfacial-driven transport phenomena do not affect the measurements of the solute diffusion coefficients in the explored concentration range.

I. INTRODUCTION

Mass transport by diffusion in a liquid mixture is often the rate-limiting step in many chemical processes and is therefore a key element in their modeling and optimization¹. Classical techniques for measuring diffusion coefficients D in liquid systems are based on the temporal monitoring of the transient relaxation of a concentration gradient in a diffusion cell using for instance interferometry^{2,3} or Raman spectroscopy⁴. However, these measurements remain tedious and also difficult because the slightest unwanted convection in the cell can dominate mass transport by diffusion.

It was recognized early that microfluidic technologies could provide adequate tools to study diffusion in liquids due to the small scales involved (10-100 μm)⁵. Many groups, for instance, performed accurate measurements of diffusion coefficients by measuring the mixing between two miscible coflowing streams in a channel, see, e.g., Refs.^{6,7} and Ref.⁸ for multicomponent mixtures. These experiments are nevertheless limited to dilute solutions (or small differences in concentration between the coflowing liquids) to avoid any coupling between flow and mass transport⁹. These measurements are also often limited to diffusion coefficients $D \geq 10^{-10} \text{ m}^2/\text{s}$, because smaller D would impose extremely small flow rates, and also small channel heights to avoid the dispersion due to the Poiseuille flow¹⁰⁻¹². Continuous on-chip electrophoresis has been developed to avoid the latter problem and thus access a wider range of D , but at the cost of being limited to electrolyte solutions¹³. Microfluidic pervaporation¹⁴, evaporation^{15,16} and ultra-filtration¹⁷ have been shown to overcome these limitations and provide diffusion coefficients even in concentrated solutions, down to $D \simeq 10^{-12} \text{ m}^2/\text{s}$. To estimate D , these experiments exploit measurements of solute concentration profiles resulting from the balance between molecular diffusion and advection by the flow induced by pervaporation, evaporation or ultra-filtration. However, these experiments require precise flow measurements and specific experimental configurations.

Few microfluidic methodologies have been developed to measure D from the temporal relaxation of a solute concentration gradient in a microchannel in the absence of convection, as in a classical diffusion cell. In particular, Culbertson *et al.* measured the diffusion coefficients of different solutes by following the time evolution of a solute plug generated by electrophoresis in a microfluidic channel¹⁸. Vogus *et al.* also measured solute diffusion coefficients by following the propagation of a diffusion front in a channel closed at one end by a hydrogel membrane to suppress convection¹⁹. Microfluidic experiments that generate a steep concentration gradient in a microchannel in the absence of flows, as in conventional diffusion cell measurements, are even more rare. Huebner *et al.*, for instance, used electrocoalescence of a pair of microdroplets immobilized in a microchannel to trigger and follow the reaction-diffusion process between these two microreservoirs of solutes²⁰. Yamada *et al.* developed an ingenious technique of removable walls in a microfluidic chamber to generate a steep concentration gradient between a solution and its solvent and follow its evolution in a static configuration²¹. More recently, Hamada *et al.* used the technique of coflowing liquids in a channel to generate a concentration gradient by stopping the flow using external valves connected to the chip²². This technique makes it possible to measure diffusion coefficients down to $D \simeq 10^{-12} \text{ m}^2/\text{s}$, mostly estimated from the long-time relaxation of the concentration gradient, when the finite size of the microfluidic channel comes into play.

In a different context, Hansen *et al.* developed microfluidic chips integrating pneumatic microvalves, commonly called Quake valves²³, to trigger the interdiffusion between a protein solution and precipitants initially separated by the valve in a channel²⁴. This technique, referred to as *free interface diffusion*²⁵, has been used to screen protein crystallization conditions at a high throughput and grow protein crystals in a convection-free environment²⁶. In the present work, we design a chip following the concept of microfluidic free interface diffusion proposed by Hansen *et al.*²⁴ that allows the generation of a steep solute concentration gradient in a

closed microchannel at a specific time. The monitoring of the transient relaxation of this gradient allows us to measure diffusion coefficients D of different solutes, over a wide range, $D \in [10^{-13} - 10^{-9}] \text{ m}^2/\text{s}$, due to the absence of convection. Beyond these measurements, we also evidence diffusio-phoresis (DP) and diffusio-osmosis (DO) phenomena^{27–29} by adding colloidal tracers in the microchannel. However, we show that these interfacial transport phenomena due to the presence of the solute concentration have no impact on the measurements presented.

II. EXPERIMENTAL SECTION

A. Chemicals and fluorescence measurements

We studied aqueous solutions of fluorescein (Sigma Aldrich) at typical concentrations of 0.03 mM and fluorescein isothiocyanate dextrans (Sigma Aldrich) with molecular weights $M_w = 4, 10, 20,$ and 70 kDa designated below as FD4, FD10, FD20, and FD70 respectively. In the latter case, the solutions were formulated by weighing with de-ionized water to achieve mass fractions $w < 0.01$. We also measured the specific volume v (m^3/kg) of aqueous solutions of dextran 70 kDa at various mass fractions and $T = 22^\circ\text{C}$, see Fig. 1 (Anton-Paar, DMA 4500). These data are well-fitted in the

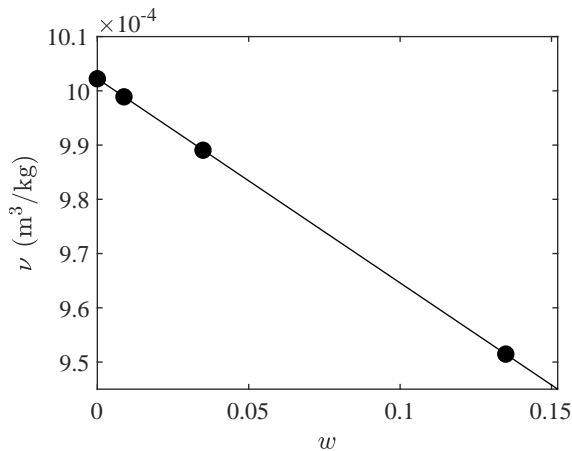


FIG. 1. Specific volume v of dextran 70 kDa solution against its mass fraction w . The continuous line is a fit by Eq. (1).

range $w = 0\text{--}0.135$ by:

$$v = v_w(1 - w) + v_d w, \quad (1)$$

with $v_w = 1.002 \times 10^{-3} \text{ m}^3/\text{kg}$ the specific volume of water at $T = 22^\circ\text{C}$ and $v_d = 6.26 \times 10^{-4} \text{ m}^3/\text{kg}$. This linear behavior shows that the volume of the water/dextran mixture does not change significantly during mixing. The fitted value v_d is in agreement with other values previously reported³⁰ and was used to convert mass fractions w of the FD solutions to volume fractions ϕ using $v\phi = v_d w$.

We also studied aqueous dispersions of fluorescent monodisperse polystyrene particles stabilized by sulfate

groups (FluoSpheres, ThermoFisher Scientific) either to track their trajectories in Sec. III B (colloid diameter $2a = 2 \mu\text{m}$) or to measure their diffusion coefficient in Sec. III C ($2a = 500 \text{ nm}$). In both cases, the dispersions were diluted sufficiently to follow the trajectories of individual particles using particle tracking algorithms³¹.

Concentration profile measurements and tracking of colloidal particles were performed using an inverted microscope (Olympus IX83) coupled to a sCMOS camera (OrcaFlash, Hamamatsu). To avoid significant photobleaching in the case of the fluorescein and FD solutions, we used a fluorescence illuminator with a shutter (X-Cite, Xylis) to limit the overall exposure during a complete experiment to a few seconds.

B. Microfluidic chip

Figure 2 shows a schematic view of the chip we developed using multilayer soft lithography to integrate pneumatically actuated valves²³. In brief, the chip is composed of two layers

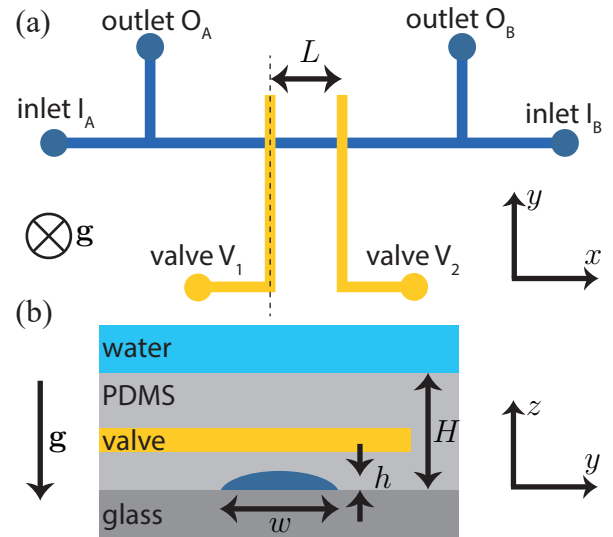


FIG. 2. (a) Schematic view of the fluidic channel network (blue) and the valves V_1 and V_2 (orange). The fluidic channel is composed of two inlets, I_A and I_B , and two outlets, O_A and O_B . In the experiments reported, the distance between the two valves is either $L = 1$ or $L = 4 \text{ mm}$. (b) Schematic cross-section of the multilevel chip along the dotted line shown in (a). To prevent pervaporation through the PDMS matrix, the chip is immersed in a water bath. The dimensions are $h = 23 \mu\text{m}$, $w = 200 \mu\text{m}$, and $H \simeq 5 \text{ mm}$. \mathbf{g} is the gravity field.

of poly(dimethylsiloxane) (PDMS) bonded to a glass slide using a plasma treatment. The first layer contains rounded channels (height $h \simeq 23 \mu\text{m}$, width $w \simeq 200 \mu\text{m}$) obtained by post heating a mold made using a positive photoresist (AZ-40XT, AZ Electronic Materials). The top PDMS layer contains two actuation rectangular channels (height $85 \mu\text{m}$, width $200 \mu\text{m}$) and is obtained from a negative photoresist mold (SU8, MicroChem). In the following experiments, the center to center distance between the two valves is either $L = 1 \text{ mm}$ or $L = 4 \text{ mm}$. The dead-end actuation channels are filled by flu-

orinated oil (Fluorinert FC-40) and connected to a pressure controller (Fluigent, MFCS-EZ). The channels containing the fluids are separated from the actuation channels by a thin layer of PDMS ($\approx 60 \mu\text{m}$) and the pressure required to completely close the valves is ≈ 1.6 bar.

C. Microfluidic protocol

Figure 3 schematically shows the protocol used to measure the diffusion coefficient of solutes in an aqueous solution. In a first step, valve V_2 is closed and the aqueous solution under study at concentration ϕ_0 and pure water are injected in the chip through inlets I_A and I_B respectively, at an imposed pressure of ≈ 300 mbar (Fluigent, MFCS-EZ). As soon as liquids flow out of outlets O_A and O_B , these are manually closed by small plugs and the gas permeability of PDMS allows the two compartments of the main channel separated by valve V_2 to be filled by both the solution and water, Fig. 3(a). Once

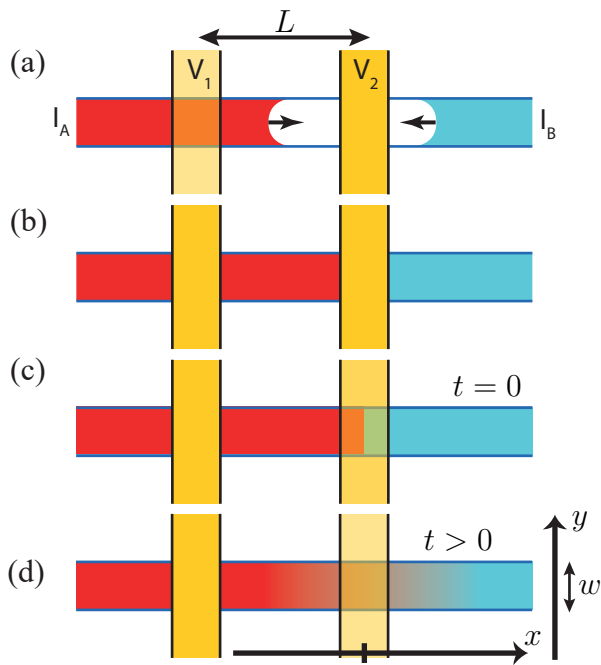


FIG. 3. Protocol for the diffusion experiments. Open valves are indicated by the transparency of the orange color indicating them. (a) The solution is injected from inlet I_A and pure water from I_B , while valve V_2 is closed. (b) Valve V_1 is then closed and valve V_2 is opened at $t = 0$ (c). (d) Diffusion in the channel closed by valve V_1 ultimately smooths the concentration gradient.

the channel is filled, the pressure at the inlets is released and valve V_1 is closed, Fig. 3(b). Valve V_2 is then opened, which leads to a steep concentration gradient between the solution and water at a well-defined time $t = 0$, Fig. 3(c). Diffusion then eventually smooths this concentration gradient at later times in the channel closed by valve V_1 , Fig. 3(d).

To evaluate the characteristic opening time of valve V_2 , we used the protocol described in Fig. 3 but with the same dilute fluorescein solution to fill the channel. The opening of

valve V_2 is then monitored using fluorescence microscopy at high frame rate, Fig. 4. The analysis of the fluorescence measured under the valve allows to estimate the opening time of this valve, $\tau \approx 200$ ms for an opening at $\approx 80\%$. This char-

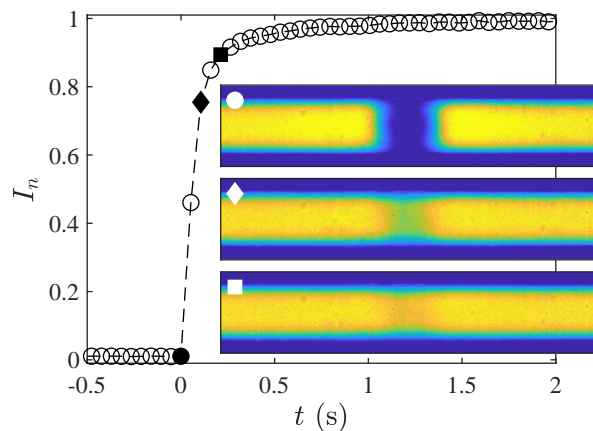


FIG. 4. Opening dynamics of valve V_2 . Both compartments are filled with the same dilute fluorescein solution. I_n is the normalized fluorescence intensity under the valve. The snapshots at $t = 0$, 106 and 212 ms show the rapid opening of the valve.

acteristic time is both related to the elasticity of the PDMS matrix and to the hydrodynamic resistance of the channel into which the volume of liquid left by the opening of valve V_2 transiently flows³². The rapid opening of the valve thus makes it possible to obtain a very steep initial solute concentration gradient using the protocol shown in Fig. 3. Indeed, molecular diffusion smooths the concentration gradient during the opening of the valve at best on a length scale $\approx \sqrt{D\tau} \approx 15 \mu\text{m}$ for a molecular solute with a diffusion coefficient $D = 10^{-9} \text{ m}^2/\text{s}$ in water.

D. Removal of pervaporation and role of free convection

In the protocol discussed above, the closed valve V_1 prevents a priori any convection in the channel and the mixing between the solution and water is thus purely diffusive. In fact, it is difficult to completely suppress all convection even in a dead-end channel because water pervaporation through the PDMS matrix inevitably induces flows in the channel^{33–35}. To illustrate this point, the water pervaporation rate q (m^2/s) per unit length can be estimated using an approximate relation derived in the case of a rectangular channel³⁶. This calculation leads to $q \approx 3 \times 10^{-13} \text{ m}^2/\text{s}$ for the geometric dimensions given in Fig. 2 and an ambient relative humidity $\text{RH} = 0.45$. The characteristic time for emptying the channel by pervaporation $\tau_p = (hw)/q$ is a few hours and not negligible compared to the relaxation time of the concentration gradient in some of the experiments discussed in this work. In order to completely eliminate pervaporation leading not only to undesirable flows, but also to the continuous accumulation by this flow of any traces of chemical species contained in the channel³⁵, the chip

is immersed in a water bath during the experiments and also a few days before to saturate the PDMS matrix with water, see Fig. 2(b)^{33,34}.

Furthermore, the difference in density between the solution and the water in the experiment shown in Fig. 3(d) also inevitably generates a flow because the density gradient is orthogonal to the gravity field \mathbf{g} . This solutal free convection flow then advects the solute and can influence the diffusive mixing between the solution and its solvent⁵. This problem has been studied recently for both the case of a microfluidic slit and a channel of rectangular cross-section³⁷. This theoretical work shows that the influence of free convection remains totally negligible for Rayleigh numbers $Ra < 10^3$, with Ra defined by:

$$Ra = \frac{\delta\rho gh^3}{\eta_w D}, \quad (2)$$

$\delta\rho$ (kg/m^3) being the density difference between water and the studied solution and η_w the water viscosity. In the experimental conditions explored in this work, $Ra \ll 10^3$, and free convection plays no role on the interdiffusion between the solution and its solvent, although the microfluidic channel is horizontal and thus orthogonal to the gravity field \mathbf{g} .

III. RESULTS

A. Molecular solutions: fluorescein and dextrans

We first applied the methodology described above in the case of dilute aqueous solutions of molecules: fluorescein and fluorescent dextrans of different molecular weights. All the measurements were performed at room temperature $T = 22^\circ\text{C}$. Figure 5 shows the results for the dextran solution of molecular weight $M_w = 4$ kDa, referred below to as FD4, the polymer volume fraction of the injected solution being $\varphi_0 \simeq 0.005$ (estimated using the measured specific volumes shown in Fig. 1).

Figure 5(a) shows the space-time plot of the fluorescence intensity profiles measured along the channel as a function of time from the opening of valve V_2 , see Fig. 3(d) for the definition of the x axis. To obtain these profiles, the fluorescence intensity was corrected by the dark value obtained when the channel is filled with water, corrected by the inhomogeneity of the UV lamp (measured when the entire channel is filled by the FD4 solution), and normalized to 1 corresponding to the intensity of the initial FD4 solution at concentration φ_0 . This space-time plot clearly shows the mutual diffusion of the polymer solution and its solvent initially separated by valve V_2 in the channel.

In such experiments, mass transport is a priori only governed by molecular Fickian diffusion because the microfluidic channel is closed by valve V_1 and pervaporation as well as solutal free convection are negligible, see Sec. IID. The volume average velocity of the binary mixture FD4 + water is therefore zero, and the polymer volume fraction follows the

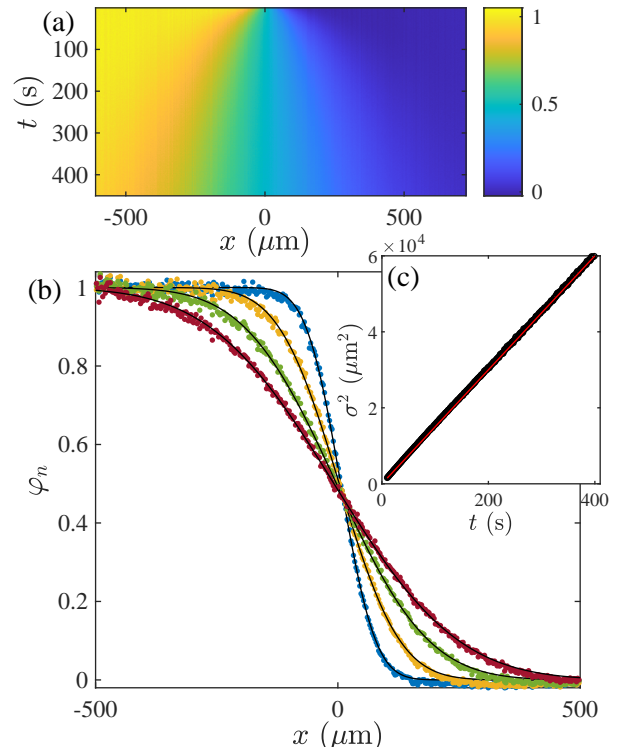


FIG. 5. Dextran diffusion. (a) Space-time plot of the normalized fluorescence profiles $\varphi_n(x,t)$ during the mutual diffusion of water and a FD4 solution (temporal resolution: one profile per second). (b) $\varphi_n(x,t)$ at $t = 10, 30, 70,$ and 130 s. The thin dark lines are fits by Eq. (4). (c) σ^2 vs t obtained from the fits of the data. The linear fit (red line) gives an estimate of the diffusion coefficient D .

diffusion equation which is in this 1D geometry¹:

$$\frac{\partial \varphi}{\partial t} = \frac{\partial}{\partial x} \left(D \frac{\partial \varphi}{\partial x} \right), \quad (3)$$

where D is the mutual diffusion coefficient of the mixture, constant for a dilute solution. This equation implies that the polymer mass transport is solely due to molecular diffusion, and thus rules out any other mechanism, such as stress gradient-induced polymer migration, see for instance^{38,39}. This hypothesis is very likely because there is no flow in the microfluidic channel closed by valve V_1 , and because it is unlikely that significant mechanical stresses were stored during the filling step described in Fig. 3 and were not released before the opening of valve V_2 .

For the initial condition, $\varphi(x < 0, t = 0) = \varphi_0$ and $\varphi(x > 0, t = 0) = 0$, the solution of Eq. (3) is⁴⁰:

$$\varphi(x,t) = \frac{\varphi_0}{2} \left[1 - \operatorname{erf} \left(\frac{x}{2\sigma} \right) \right], \quad (4)$$

where $\sigma = \sqrt{Dt}$ is the width of the diffusion zone. For this result, we implicitly assume an infinite geometry along x , and Eq. (4) is in fact only valid for $t \ll L^2/D$, where L is the distance between the two valves ($L^2/D \simeq 4$ h for $L = 4$ mm and $D = 10^{-9}$ m^2/s). Figure 5(b) shows that $\varphi_n = \varphi(x,t)/\varphi_0$ given

TABLE I. Molecular weight M_w of the different solutes studied and measured diffusion coefficients D in water.

Solutes	Fluorescein	FD4	FD10	FD20	FD70
M_w (g/mol)	332	4000	10000	20000	70000
$D \times 10^{10}$ (m ² /s)	4.5	1.6	1.0	0.9	0.46

by Eq. (4) perfectly fits the measured normalized intensity profiles validating the above assumptions and further showing that the fluorescence intensity varies linearly with ϕ under these dilute conditions. The linear behavior σ^2 vs t shown in Fig. 5(c) leads to $D \simeq 1.6 \times 10^{-10}$ m²/s.

We performed these same measurements for dilute aqueous solutions of fluorescein and FD of higher molecular weights up to $M_w = 70$ kDa. For all these experiments, Eq. (4) correctly fits the 1D fluorescence intensity profiles and the linear behaviors σ^2 vs t lead to precise estimates of the diffusion coefficients D , see the inset of Fig. 6. The corresponding D values given in Table I are also plotted in Fig. 6 against M_w . These values are in agreement with other reported data mea-

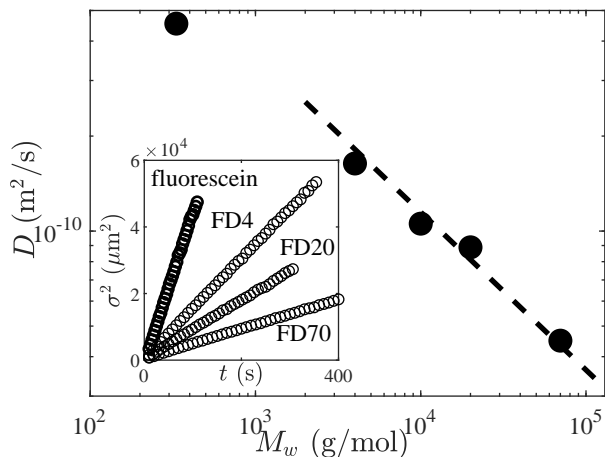


FIG. 6. Measured diffusion coefficients D vs molecular weights M_w of the solutes considered (fluorescein, dextran FD4, FD10, FD20, and FD70), see Table I. The dotted line shows the scaling behavior $D \sim 1/\sqrt{M_w}$ for the dextrans. The inset shows the corresponding curves σ^2 vs t from which D are estimated by linear fits (the FD10 case is not shown for clarity).

sured using the temporal widening of a fluorescein plug in a microchannel¹⁸ and by modulated fringe pattern photobleaching for the FD solutions⁴¹. The scaling law $D \sim M_w^{-1/2}$ shown in Fig. 6 and also reported in Ref.⁴¹ is coherent with the random coil conformation of dextran molecules in water. Indeed, for a loose polymer conformation, one expects that the radius of gyration follows $R_g \sim \sqrt{M_w}$, and according to the Stokes-Einstein relation, $D \sim 1/R_h \sim 1/\sqrt{M_w}$ where $R_h \sim R_g$ is the hydrodynamic radius of the dextran coil in water⁴¹.

B. Evidence of diffusio-phoresis and diffusio-osmosis

The results presented above, in particular the correct description of the temporal widening of the concentration gradient by Eq. (4) with $\sigma = \sqrt{Dt}$, suggest that the solute transport is governed by diffusion only. To confirm this hypothesis, we added fluorescent colloids (diameter $2a = 2 \mu\text{m}$) to the FD70 solution and tracked their positions, x_c vs t , along with the relaxation of the polymer concentration gradient. Strikingly, these experiments reveal that the colloids, in addition to their Brownian motion, move towards the low polymer concentration, see Fig. 7 for an experiment at $\phi_0 = 0.005$ (multimedia view).

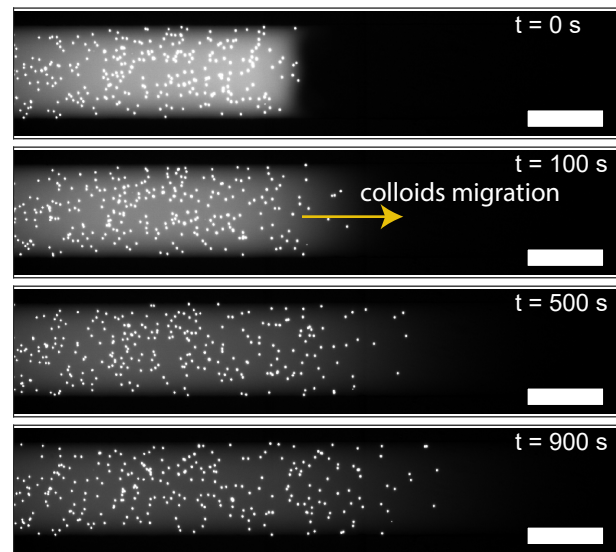


FIG. 7. Fluorescence snapshots showing the temporal relaxation of a concentration gradient of FD70 with fluorescent colloids dispersed in the polymer solution. The colloids migrate to the low polymer concentration (see the arrow), because of diffusio-phoresis induced by the polymer concentration gradient, see Sec. III B 1. Scale bar: 100 μm (multimedia view).

To better visualize these displacements, Fig. 8 shows the relative displacement at $t = 840$ s of each colloid from its initial position $\delta x = x_c(t) - x_0$ as a function of $x_0 = x_c(t = 0)$. At this time, the width of the polymer diffusion zone is $\sigma = \sqrt{Dt} \simeq 200 \mu\text{m}$. We have retained in this analysis only colloids initially away from the channel edges ($\|y\| < w/2 - 20 \mu\text{m}$), in order to avoid possible confinement effects related to the rounded shape of the channel. These data help to reveal that the colloid movement is correlated to the polymer gradient: particles initially upstream of the initial concentration gradient ($x_0 < -\sigma$) show very little displacements, while particles initially close to $x = 0$ show displacements that can reach $\delta x \simeq 250 \mu\text{m}$. Figure 8 also shows the same data but for colloids dispersed in pure water only, showing in this case $\delta x \simeq 0$ with deviations that can be explained by Brownian motion, $\sqrt{D_{SD}t} \simeq 15 \mu\text{m}$, with $D_{SD} \simeq 2.2 \times 10^{-13}$ m²/s the colloid self-diffusion coefficient estimated using the Stokes-Einstein relation.

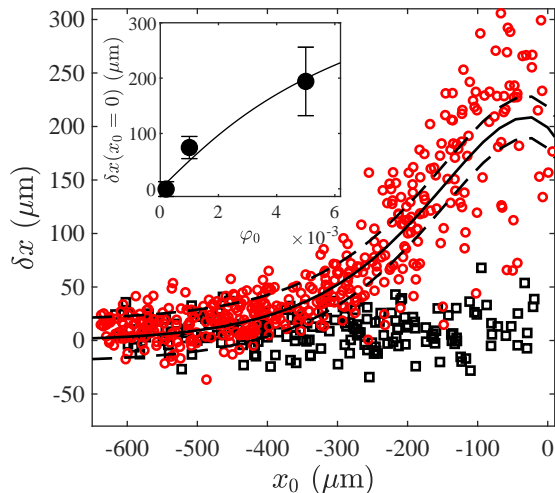


FIG. 8. Colloid displacements δx at $t = 840$ s vs their initial positions x_0 . Red circles: mutual diffusion of water and FD70 at concentration $\phi_0 = 0.005$ with dispersed colloids; black squares: colloid displacements in the absence of FD (diffusion in pure water). The continuous line is the prediction by the solution of Eq. (6). The two dashed lines show the Brownian dispersion $\pm\sqrt{2D_{SD}t}$. Inset: displacement δx at $t = 840$ s for the colloids initially located at $x_0 \simeq 0$ vs initial volume fraction ϕ_0 of the FD70 solution. The errorbars are the standard deviations of the data. The solid line is the prediction given by Eq. (9).

These observations point to the phenomena of diffusio-phoresis (DP) and diffusio-osmosis (DO). These interfacial fluid transport phenomena are due to specific interactions between the solute (FD polymers) and solid surfaces, that occur in a diffuse layer of small thickness either at the colloid surface or the channel walls²⁷⁻²⁹. The solute concentration gradient induces a pressure gradient in the diffuse layer (parallel to the interface) which is mechanically balanced by a viscous stress leading either to the net movement of freely suspended colloids (DP) or to a bulk flow in the channel (DO). Such phenomena have been reported many times, in particular for electrolytes as solutes⁴²⁻⁴⁸, with a wide range of possible applications^{29,49}, including microfluidics⁵⁰⁻⁵³. In the case of neutral solutes, small molecules but also polymers⁵⁴⁻⁵⁹, studies are scarcer and comparisons with theoretical models still raise issues^{56,59}. This last case is also key to the understanding of other phenomena such as the stratification observed during the drying of colloidal films⁶⁰⁻⁶⁴.

Our aim here is not to study these phenomena as such, but to show that the measured colloid displacements are consistent with DP induced by the dextran gradient and that DO probably also occurs simultaneously, explaining the deviations of the data shown in Fig. 8. We also show below that diffusio-osmotic flows do not a priori impact the D measurements presented in Sec. III A.

1. Diffusio-phoresis induced by the dextran concentration gradient

For simplicity, we assume the Asakura-Oosawa model for the FD solution^{57,60}: (i) no polymer-polymer interactions at the volume fractions ϕ considered and (ii) polymer chains excluded from the colloid surface on a length scale $R_i \ll a$, therefore behaving as "hard-spheres". In this model, the DP drift velocity of a colloidal particle in the FD gradient is given by:

$$v_{DP} = -\frac{R_i^2 k_B T}{2\eta_w} \nabla n, \quad (5)$$

with k_B the Boltzmann constant and n the number density of polymer chains ($\#/m^3$). For the FD70 solution, n is estimated by $n = \phi/\bar{v}_d$ with $\bar{v}_d = M_w v_d/\mathcal{N}_a$ the molecular volume of FD, \mathcal{N}_a the Avogadro number, $M_w = 70$ kg/mol, and $v_d = 6.26 \times 10^{-4}$ m³/kg the specific volume in Eq. (1). This is obviously a rough estimate that ignores, for example, the molecular weight distribution of the polymer sample.

Following Eq. (4) and Eq. (5), the trajectory of a colloidal particle x_c vs t due to DP when neglecting its Brownian motion is given by the solution of the ordinary differential equation:

$$\frac{dx_c}{dt} = v_{DP}(x_c(t), t) = \frac{R_i^2 k_B T \phi_0}{2\eta_w \bar{v}_d} \frac{e^{-\frac{x_c^2}{4t}}}{\sqrt{4\pi Dt}}, \quad (6)$$

with ϕ_0 the volume fraction of the initially injected FD solution. With the dimensionless variables $\tilde{x}_c = x_c/h$ and $\tilde{t} = Dt/h^2$, Eq. (6) becomes

$$\frac{d\tilde{x}_c}{d\tilde{t}} = \phi_0 \Gamma \frac{e^{-\frac{\tilde{x}_c^2}{\tilde{t}}}}{\sqrt{\tilde{t}}}, \quad (7)$$

with

$$\Gamma = \frac{3\sqrt{\pi} R_{SE} R_i^2}{2 \bar{v}_d}, \quad (8)$$

and $R_{SE} \simeq 4.9$ nm the Stokes-Einstein radius of the FD70 polymer particles defined by $D = k_B T / (6\pi\eta_w R_{SE})$. In the model of spherical "hard-sphere" colloids considered in Ref.⁶⁰, $R_i = R_{SE}$ and $\bar{v}_d = 4\pi R_{SE}^3/3$ so that $\Gamma = 9/(8\sqrt{\pi}) \simeq 0.63$. In this case, Eq. (7) and the assumption of dilute solution $\phi_0 \ll 1$ necessarily impose a small DP velocity.

In the FD70 case shown in Fig. 8, however, the best fit of the experimental data is obtained by the numerical solutions of Eq. (6) for $R_i = 27$ nm, and thus for a relatively large interaction radius compared to R_{SE} ($\Gamma \gg 1$). Such a value is in agreement with previously reported data by Staffeld and Quinn who found $R_i \simeq 38$ nm also for dextran in water ($M_w = 40$ kg/mol, $R_{SE} = 4.8$ nm)⁵⁷. The fact that R_i is significantly larger than R_{SE} was interpreted by Staffeld and Quinn as being due to the flexible conformation of the dextran coil in water⁵⁷. As discussed later on, this large difference remains surprising and raises questions, because other studies have reported $R_i \simeq R_{SE}$ for polyethylene glycol polymers (PEG) using a different experimental configuration: DO in nanochannels^{58,59}.

Equation (7) also shows that the magnitude of DP a priori depends on the initial polymer concentration ϕ_0 . The inset of Fig. 8 confirms this result by showing the relative displacement δx at $t = 840$ s of colloids that were close to the initial concentration gradient at $t = 0$ ($x_0 \in [-h; 0]$) for three different initial volume fractions of FD70 solutions ($\phi_0 = 2 \times 10^{-4}$, 1×10^{-3} , and 5×10^{-3}). Moreover, Eq. (7) admits a self-similar solution for the initial condition $x_0 = 0$, which leads to:

$$x_c = \sqrt{2W(2\phi_0^2\Gamma^2)Dt}, \quad (9)$$

W being the Lambert function. As shown in the inset of Fig. 8, Eq. (9) correctly fits the results with the same parameters as above ($R_i = 27$ nm). Equation (9) also shows that the colloids always remain "slaves" of the polymer diffusion in such experiments, even for possibly high ϕ_0 or Γ values (high R_i), because of the slow logarithmic increase of the Lambert function in Eq. (9). This specificity and the effective diffusive behavior given by Eq. (9) are somehow similar to results derived by Abécassis *et al.* for colloid DP induced by salt concentration gradients in coflow microfluidic experiments^{43,50}. Because the colloid dynamics is slaved to solute diffusion, these experiments are not the most appropriate for quantitatively studying DP transport, in particular Eq. (5), compared to experiments that track colloid trajectories in an independently imposed steady solute gradient as, for instance, in Refs.^{48,52,54,56}.

2. Possible role of diffusio-osmosis

Even if the aforementioned model roughly describes our observations in quantitative agreement with previously reported data⁵⁷, it cannot explain the large deviations in displacements shown in Fig. 8, which cannot be accounted for by the Brownian motion alone. By changing the focal plane of the microscope during the relaxation of the polymer gradient, it appears that the colloid drift velocity also slightly depends on the altitude z in the channel.

These observation possibly suggest the simultaneous development of DO within the channel due to the specific interaction of the polymer with the channel walls, as observed by other groups using micro- and nanofluidic experiments for other neutral solutes, PEG^{58,59} and glucose⁵⁶. Indeed, if the polymer chains are excluded from the channel walls on a given length scale, we also expect an apparent slip velocity v_s , given similarly to DP by Eq. (5), but with opposite sign, the fluid flow being directed toward the high polymer concentration. Because of the volume continuity, these slip velocities induce a recirculating flow in the channel directly correlated with the polymer concentration gradient, even if the channel is closed by valve V_1 , see Fig. 9 for a schematic cross-sectional view in the case of a 2D slit. Colloids dispersed in the polymer solution are then subject to two transport mechanisms (diffusion in dead-end pores) but for electrolyte solutions⁴⁵⁻⁴⁷: migration by DP and advection by DO, and the resulting colloid drift velocity can then depend on z .

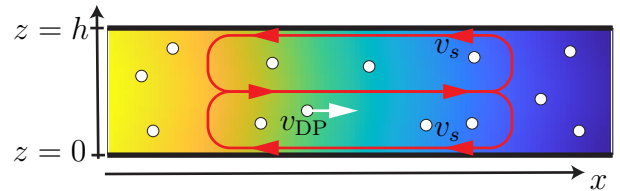


FIG. 9. Superposition of DO (red) and colloid DP (white) in a channel of height h . The polymer concentration gradient is shown by the color gradient.

Our data also suggest that DO and DP have the same order of magnitude, i.e., $v_s \simeq -v_{DP}$, see schematically Fig. 9. Indeed, if DO dominated DP, then we would have observed colloids transported to both the high and low polymer concentration (depending on z , see Fig. 9), whereas if DP dominated DO, we would not have observed the large dispersion of the data shown in Fig. 8. Only time-resolved confocal fluorescence microscopy (due to the transient relaxation of the concentration gradient) would allow us to probe quantitatively the 3D flow and thus disentangle the contributions due to DO and DP to colloid movements. These difficult measurements, recently done by Williams *et al.*⁵⁶ to disentangle DO from buoyancy-driven convection in their case, are, however, beyond the scope of this work. They remain, nevertheless, necessary for a quantitative understanding of these interfacial-driven transport phenomena, and might explain in particular, why R_i estimated in Sec. III B 1 but also in Ref.⁵⁷ by considering only DP is significantly larger than R_{SE} for dextran, whereas other experiments have reported $R_i \simeq R_{SE}$ for DO induced by PEG gradients in nanochannels^{58,59}.

Furthermore, it is legitimate to ask whether the presence of DO in the channel, induced by the polymer concentration gradient, may impact the transport of the polymer itself (by advection) in the diffusion experiments presented in Sec. III A. To address this question, we first consider for simplicity the case of a 2D slit of height h as in Fig. 9. The rounded shape of the fluidic channel would indeed require numerical tools to compute the 3D flow. We then assume that the polymer concentration gradient at the walls ($z = 0$ and $z = h$) induces a DO slip velocity $v_s = -v_{DP}$, with v_{DP} given by Eq. (5). The Péclet number $Pe = v_s h / D$ allows to compare the polymer diffusion and its advection by DO. The D measurements shown previously are a priori only valid when the polymer advection is negligible, i.e., when $Pe \ll 1$. To go beyond this scaling analysis and also take into account the dependence of v_s with the polymer concentration gradient, we performed an analysis similar to the Taylor-Aris dispersion, see the review in Ref.⁶⁵ on solute dispersion in shear flows. In this framework, we showed in Appendix A using the lubrication approximation that the height-averaged polymer concentration $\langle \phi \rangle$ follows:

$$\frac{\partial \langle \phi \rangle}{\partial t} = \frac{\partial}{\partial x} \left(D_{\text{eff}} \frac{\partial \langle \phi \rangle}{\partial x} \right), \quad (10)$$

with

$$D_{\text{eff}} = D \left[1 + \frac{2\pi\Gamma^2 h^2}{105} \left(\frac{\partial \langle \phi \rangle}{\partial x} \right)^2 \right]. \quad (11)$$

The dispersion term in Eq. (11) accounts for advection of the polymer by DO, the non-linearity coming from the dependence of the magnitude of DO with the polymer gradient unlike the classical Taylor-Aris problem. The same non-linearity occurs for the dispersion of a buoyant solute in a horizontal channel, as solutal free convection likewise depends on the magnitude of the concentration gradient, see, e.g., Ref.³⁷. In our experiments, the highest expected dispersion ($\varphi_0 = 0.005$ and $\sigma \sim h$) is about:

$$D_{\text{eff}} \simeq D \left(1 + \frac{2\pi\Gamma^2\varphi_0^2}{105} \right) \simeq 1.03D, \quad (12)$$

and diffusion thus always dominates the relaxation of the polymer gradient despite DO in the channel. The aforementioned relationship suggests, however, that dispersion of the polymer by DO generated itself by the polymer gradient may occur for a higher concentration, nevertheless challenging the assumption of dilute solution.

C. Colloidal dispersions

We have demonstrated in Sec. III A that the microfluidic experiments shown in Fig. 3 can be used to measure molecular diffusion coefficients in the range $D \in [0.5 - 5] \times 10^{-10}$ m²/s. To show that the same methodology can also be used to measure much smaller diffusion coefficients, we performed similar experiments, but for dilute dispersions of colloids of radius $a = 250$ nm.

To measure the 1D colloidal concentration field $\varphi(x, t)$, we studied dispersions of fluorescent colloids diluted enough with pure water (typically $\simeq 10^{15}$ colloids/m³) to be able to directly count the colloids and thus their density along the channel with a good accuracy, see Fig. 10(a). As for the FD and fluorescein cases, these concentration profiles are normalized by 1, but Eq. (4) does not capture the temporal relaxation of the colloid concentration gradient, see Fig. 10(a). However, we found that the relation:

$$\varphi_n(x, t) = \frac{1}{2} \left[1 - \text{erf} \left(\frac{x - c}{2\sigma} \right) \right], \quad (13)$$

correctly fits the data, c and σ being free parameters. The space-time diagram shown in Fig. 10(b) corresponding to these fits clearly shows an overall convective motion, directed toward the high colloid concentrations, superimposed on the broadening of the mixing zone by diffusion. Figure 10(c) shows that the width of the mixing zone σ follows $\sigma^2 = Dt$ leading to an estimate of the colloid diffusion coefficient $D \simeq 6.7 \times 10^{-13}$ m²/s. For this experiment, the distance between the two valves (see Fig. 2) is $L = 4$ mm and the data c vs t plotted in Fig. 10(d) show a global displacement of the diffusion zone of $\simeq 200$ μm in $\simeq 600$ min that gradually slows down.

We believe this very weak convective motion is due to colloid DP due to the relaxation of a molecular solute gradient present in minute amounts, simultaneously with colloid diffusion. Indeed, the commercial colloidal dispersion contains

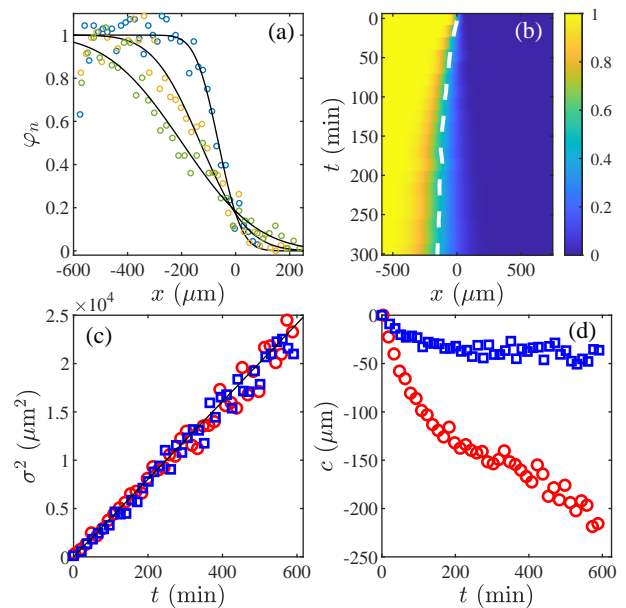


FIG. 10. Colloid diffusion. (a) Experimental normalized concentration profiles $\varphi_n(x, t)$ at $t = 63, 213,$ and 588 min. The dark lines are fits by Eq. (13). (b) Space-time plot of the fitted profiles for $L = 4$ mm. The dotted line, c vs t , shows the shift of the center of the diffusion zone. (c) σ^2 vs t and (d) c vs t for two different experiments: $L = 1$ mm (blue square) and $L = 4$ mm (red circles). The linear fit in (c) gives $D \simeq 6.7 \times 10^{-13}$ m²/s.

traces of surfactants or ionic solutes such as sodium azide as a preservative, that can induce DP, toward the high solute concentration in our experiments, as shown in many experiments reporting colloid DP in solutions of electrolytes^{43,45}. To test this assumption, we performed the same experiments but with a new chip for which the distance between the two valves is now $L = 1$ mm. Again, the concentration profiles are well-fitted by Eq. (13) and the width of the diffusion zone follows $\sigma^2 = Dt$ with the same D value, see Fig. 10(c). In this case, however, the shift c vs t reaches for $t \simeq 100$ min a small plateau value $c \simeq -40$ μm , see Fig. 10(d). We believe that this quantitatively different behavior is due to the relaxation by diffusion of the concentration gradient of the molecular impurity responsible for the colloid DP. Indeed, the initial volume of the dispersion is defined in our protocol by the distance L between the two valves, see Fig. 3. The concentration gradient of the impurity initially contained in the dispersion relaxes on a timescale $\sim L^2/D_i$ with D_i its diffusion coefficient. For $D_i \simeq 5 \times 10^{-10}$ m²/s, $L^2/D_i \simeq 30$ min for $L = 1$ mm and is 16 times smaller than the $L = 4$ mm case ($L^2/D_i \simeq 530$ min). These simple arguments allow us to account, at least qualitatively, for the behaviors shown in Fig. 10(d), and also show how the distance L between the valves can be adapted to avoid colloid DP (with the assumption $D \ll D_i$). Another possibility to get rid of DP would be to intentionally add salts at the same concentration to both the initial water and dispersion reservoirs to saturate any ionic impurity background initially present in the dispersion. In the case of concentrated colloidal dispersions, this strategy could on the other hand modify the

colloidal interactions and thus the measured diffusion coefficient⁶⁶.

The aforementioned experiments lead to a precise estimate of the diffusion coefficient of the colloids $D \simeq 6.7 \pm 0.3 \times 10^{-13}$ m²/s, the errorbar corresponding to the deviation over several experiments. This value, estimated from the relaxation of a colloid concentration gradient over long time scales ($\simeq 600$ min) is known as the mutual or long-time collective diffusion coefficient⁶⁶. For comparison, we also measured the self-diffusion coefficient D_{SD} of the same colloids, tracking their mean square displacements on short time scales (a few seconds), see Appendix B. These measurements lead to $D_{SD} \simeq 7.9 \pm 0.5 \times 10^{-13}$ m²/s corresponding to a colloid radius $a \simeq 270 \pm 15$ nm using the Stokes-Einstein relation at $T = 22^\circ\text{C}$ (manufacturer data, $a = 250$ nm). For this dilute dispersion, we expect $D \simeq D_{SD}$ because both colloidal and hydrodynamic interactions are a priori negligible⁶⁶. The slight measured difference ($\simeq 15\%$) may be due to our too rough estimation of D_{SD} from the colloid mean square displacements (see Appendix B), or to experimental artifacts in our measurements of the colloid concentration profiles due to the unavoidable adhesion of some colloids to the channel walls on long time scales. This slight difference could also be due to more subtle effects such as the confinement of the colloids in the channel, especially near the edges due to its rounded shape which may modify their self-diffusivity⁶⁷, see Ref.⁶⁸ for the case of charged colloids.

IV. CONCLUSIONS

In this work, we have developed a microfluidic chip to track the relaxation of a steep solute concentration gradient in a microchannel closed to suppress convection. In the case of dilute solutions and colloidal dispersions, this methodology allowed us to measure solute diffusion coefficients over a very wide range, $D \in [10^{-13} - 10^{-9}]$ m²/s, without convection disturbance. Due to the high control of the mass transport conditions at these small scales, these experiments also revealed interfacial-driven transport phenomena, colloid DP and DO, due to the presence of the solute concentration gradient. We have nevertheless shown that these transport phenomena do not interfere with the D measurements made under our conditions. These experiments could in turn provide new data on these phenomena, especially in the case of neutral solute, if one is able to disentangle transport due to DP and DO using for instance time-resolved confocal microscopy or chemical modifications of the channel walls or colloid surfaces to suppress either DP or DO.

The methodology described in the present work could also be useful for probing mutual (collective) diffusion in more concentrated systems, for which solute-solute and hydrodynamic interactions are expected to play a role⁶⁶. In the case of charged colloidal dispersions containing both salts and colloids, being able to adjust the distance L between the valves to decouple the diffusion of salts from that of colloids (see Sec. III C) is a major asset not only for measuring the collective diffusion coefficient of dispersions in equilibrium with a

reservoir of known ionic content¹⁷, but also for tackling the complexity of mass diffusion in such systems⁶⁹. Finally, the permeation property of the PDMS matrix of the chip could also be exploited to concentrate solutes in the channel by per-vaporation³⁵, prior the diffusion experiment triggered by the opening of valve V_2 , see Fig. 3. Such experiments would then allow to probe the phenomenon of mutual diffusion using the technique of microfluidic free interface diffusion, even in the case of highly concentrated solutions or dispersions.

Appendix A: Solute dispersion by diffusio-osmosis

We consider the experiments described in Sec. III A but for a 2D slit of height h . At the microfluidic scales ($h \simeq 23$ μm in the experiments), inertia is totally negligible and the dispersion of the solute by free convection can also be neglected³⁷. The equations governing the polymer volume fraction and the flow are thus:

$$\frac{\partial \varphi}{\partial t} + \mathbf{v} \cdot \nabla \varphi = D \Delta \varphi, \quad (\text{A1})$$

$$\nabla \cdot \mathbf{v} = 0, \quad (\text{A2})$$

$$\eta_w \Delta \mathbf{v} = \nabla p. \quad (\text{A3})$$

where \mathbf{v} is the flow due to DO induced by the polymer concentration gradient, and p is the pressure field. We assumed above that the polymer solution is dilute with a constant viscosity η_w . DO arises because of the repulsion of the polymer chains from the walls of the slit, which results in the following slip velocity:

$$v_x(z=0 \text{ and } h) = \frac{k_B T R_i^2}{2 \eta_w \bar{v}_d} \left(\frac{\partial \varphi}{\partial x} \right)_{z=0, h}, \quad (\text{A4})$$

which is similar to Eq. (5) corresponding to DP of a colloidal particle in the polymer gradient. With the dimensionless variables:

$$\begin{aligned} \tilde{t} &= Dt/h^2, \quad \tilde{x} = x/h, \quad \tilde{\mathbf{v}} = h\mathbf{v}/D, \\ \tilde{p} &= h^2 p / (\eta_w D), \quad \tilde{\varphi} = \varphi / \varphi_0, \end{aligned} \quad (\text{A5})$$

the aforementioned model reads:

$$\frac{\partial \tilde{\varphi}}{\partial \tilde{t}} + \tilde{\mathbf{v}} \cdot \nabla \tilde{\varphi} = \Delta \tilde{\varphi}, \quad (\text{A6})$$

$$\nabla \cdot \tilde{\mathbf{v}} = 0, \quad (\text{A7})$$

$$\Delta \tilde{\mathbf{v}} = \nabla \tilde{p}, \quad (\text{A8})$$

and:

$$\tilde{v}_x(\tilde{z} = 0 \text{ and } \tilde{z} = 1) = 2\sqrt{\pi} \varphi_0 \Gamma \left(\frac{\partial \tilde{\varphi}}{\partial \tilde{x}} \right)_{\tilde{z}=0,1}. \quad (\text{A9})$$

We now assume:

$$\tilde{\varphi}(\tilde{x}, \tilde{z}, \tilde{t}) = \langle \tilde{\varphi} \rangle(\tilde{x}, \tilde{t}) + \tilde{\varphi}_1(\tilde{x}, \tilde{z}, \tilde{t}), \quad (\text{A10})$$

with $\langle \tilde{\varphi} \rangle$ the height-averaged concentration defined by:

$$\langle \tilde{\varphi} \rangle = \int_0^1 \tilde{\varphi}(\tilde{x}, \tilde{z}, \tilde{t}) d\tilde{z}, \quad (\text{A11})$$

and $\tilde{\varphi}_1 \ll \langle \tilde{\varphi} \rangle$. Averaging of the transport equation Eq. (A6) over the height of the slit with the help of Eq. (A7) leads to:

$$\frac{\partial \langle \tilde{\varphi} \rangle}{\partial \tilde{t}} + \frac{\partial \langle \tilde{v}_x \tilde{\varphi}_1 \rangle}{\partial \tilde{x}} = \frac{\partial^2 \langle \tilde{\varphi} \rangle}{\partial \tilde{x}^2}. \quad (\text{A12})$$

In the framework of the lubrication approximation, i.e., for a polymer concentration gradient extended over a length scale $\gg 1$, one can show by subtracting Eq. (A12) to the transport equation Eq. (A6) that we get:

$$\tilde{v}_x \frac{\partial \langle \tilde{\varphi} \rangle}{\partial \tilde{x}} \simeq \frac{\partial^2 \tilde{\varphi}_1}{\partial \tilde{z}^2}, \quad (\text{A13})$$

for $t \gg 1$, see Ref.⁶⁵ on solute dispersion in shear flows for more details on such calculations. Similarly, it can be shown, still within the lubrication approximation, that the x -component of the velocity field is given by:

$$\tilde{v}_x \simeq 2\sqrt{\pi}\varphi_0\Gamma \frac{\partial \langle \tilde{\varphi} \rangle}{\partial \tilde{x}} (6\tilde{z}^2 - 6\tilde{z} + 1). \quad (\text{A14})$$

Equation (A13) along with Eq. (A14) and the impermeability conditions at the walls can be used to compute $\tilde{\varphi}_1$:

$$\tilde{\varphi}_1 = 2\sqrt{\pi}\varphi_0\Gamma \left(\frac{\partial \langle \tilde{\varphi} \rangle}{\partial \tilde{x}} \right)^2 \left(\frac{\tilde{z}^4}{2} - \tilde{z}^3 + \frac{\tilde{z}^2}{2} - \frac{1}{60} \right). \quad (\text{A15})$$

Equations (A15) and (A14) can then be used to calculate the dispersion term in Eq. (A12) leading to Eq. (10) with real units. Similar calculations are also derived and discussed in detail in Ref.³⁷ dealing with solute dispersion due to free convection in a microfluidic slit.

Appendix B: Colloid self-diffusion coefficient

To estimate the self-diffusion coefficient of the colloids, we first filled the entire microfluidic channel with the dispersion used in the experiments described in Sec. III C at a higher dilution ($\simeq 5 \times 10^{13}$ colloids/m³) and then closed valve V₁. We then acquired images for $\simeq 1$ h on a field of view of $\simeq w \times w$, w being the channel width. Two-dimensional trajectories of the colloids were extracted from the image stack using standard particle tracking algorithms³¹, see Fig. 11(a). From about 50 trajectories, we then computed the mean square displacement $\langle x^2 \rangle$ and $\langle y^2 \rangle$ against time τ . Figure 11(b) shows that $\langle x^2 \rangle \simeq \langle y^2 \rangle = 2D_{\text{SD}}\tau$ with $D_{\text{SD}} \simeq 7.9 \pm 0.5 \times 10^{-13}$ m²/s, the standard deviation being calculated from the deviation over the different trajectories.

These measurements of the self-diffusion coefficient would deserve a finer estimation and more discussion⁷⁰, notably on the number of trajectories followed, the precision on the localization of the particles, the statistical estimation of D_{SD} from the trajectories⁷¹, the size distribution of the tracers, the role of confinement⁶⁷, see also Ref.⁶⁸ for the case of charged colloids, etc.

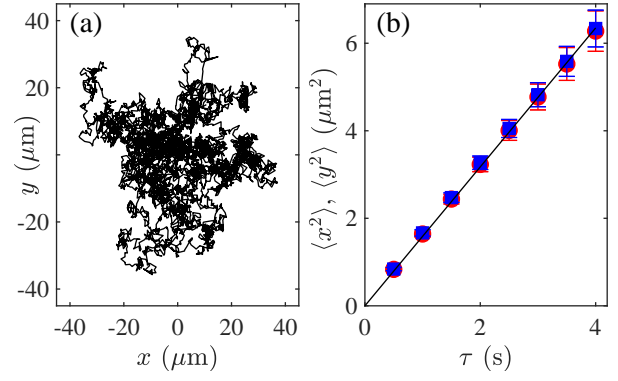


FIG. 11. (a) Example of a colloid trajectory in the x - y plane. (b) Mean square displacement of the colloids vs time τ (blue squares: x -direction, red bullets: y -direction). The errorbars are estimated from the deviation over $\simeq 50$ different trajectories. The solid line is the best fit by $\langle x^2 \rangle = \langle y^2 \rangle = 2D_{\text{SD}}\tau$

ACKNOWLEDGMENTS

We thank C. Ybert for his insightful comments. We also acknowledge Solvay, CNRS and the ANR program Grant No. ANR-18-CE06-0021 for financial support.

- ¹E. L. Cussler, *Diffusion : Mass Transfer in Fluid Systems* (Cambridge University Press, 1997).
- ²J. M. Creeth, "Studies of Free Diffusion in Liquids with the Rayleigh Method. I. The Determination of Differential Diffusion Coefficients in Concentration-dependent Systems of Two Components," *J. Am. Chem. Soc.* **77**, 6428 (1955).
- ³C. S. Caldwell, J. R. Hall, and A. L. Babb, "Mach-Zehnder Interferometer for Diffusion Measurements in Volatile Liquid Systems," *Rev. Sci. Instrum.* **28**, 816 (1957).
- ⁴A. Bardow, V. Goke, H. J. Koß, K. Lucas, and W. Marquardt, "Concentration-dependent diffusion coefficients from a single experiment using model-based Raman spectroscopy," *Fluid Phase Equilib.* **228-229**, 357 (2005).
- ⁵T. M. Squires and S. R. Quake, "Microfluidics: fluid physics at the nanoliter scale," *Rev. Mod. Phys.* **77**, 977 (2005).
- ⁶A. E. Kamholz, E. A. Schilling, and P. Yager, "Optical measurement of transverse molecular diffusion in a microchannel," *Biophysical J.* **80**, 1967 (2001).
- ⁷J.-B. Salmon, A. Ajdari, P. Tabeling, L. Servant, D. Talaga, and M. Joanicot, "In situ Raman imaging of interdiffusion in a microchannel," *Appl. Phys. Lett.* **86** (2005).
- ⁸C. Peters, L. Wolff, S. Haase, J. Thien, T. Brands, H.-J. Koß, and A. Bardow, "Multicomponent diffusion coefficients from microfluidics using Raman microspectroscopy," *Lab Chip* **17**, 2768 (2017).
- ⁹J. Dambrine, B. Géraud, and J.-B. Salmon, "Interdiffusion of liquids of different viscosities in a microchannel," *New J. Phys.* **11**, 075015 (2009).
- ¹⁰R. F. Ismagilov, A. D. Stroock, P. J. A. Kenis, G. M. Whitesides, and H. A. Stone, "Experimental and theoretical scaling laws for transverse diffusive broadening in two-phase laminar flows in microchannels," *Appl. Phys. Lett.* **76**, 2376 (1999).
- ¹¹A. E. Kamholz and P. Yager, "Molecular diffusive scaling laws in pressure-driven microfluidic channels: deviation from onedimensional Einstein approximations," *Sensors and Actuators B* **82**, 117 (2000).
- ¹²J.-B. Salmon and A. Ajdari, "Transverse transport of solutes between co-flowing pressure-driven streams for microfluidic studies of diffusion/reaction processes," *J. Appl. Phys.* **101**, 074902 (2007).
- ¹³A. Estevez-Torres, C. Gosse, T. LeSaux, J. F. Allemand, V. Croquette, H. Berthoumieux, A. Lemarchand, and L. Jullien, "Fourier Analysis To

- Measure Diffusion Coefficients and Resolve Mixtures on a Continuous Electrophoresis Chip,” *Anal. Chem.* **79**, 8222 (2007).
- ¹⁴A. Bouchaudy, C. Loussert, and J.-B. Salmon, “Steady microfluidic measurements of mutual diffusion coefficients of liquid binary mixtures,” *AIChE* **64**, 358 (2018).
- ¹⁵L. Goehring, J. Li, and P.-C. Kiatkirakajorn, “Drying paint: from micro-scale dynamics to mechanical instabilities,” *Phil. Trans. R. Soc. A* **375**, 20160161 (2017).
- ¹⁶K. Roger, E. Sparr, and H. Wennerström, “Evaporation, diffusion and self-assembly at drying interfaces,” *Phys. Chem. Chem. Phys.* **20**, 10430 (2018).
- ¹⁷C. Keita, Y. Hallez, and J.-B. Salmon, “Microfluidic osmotic compression of a charge-stabilized colloidal dispersion: Equation of state and collective diffusion coefficient,” *Phys. Rev. E* **104**, L062601 (2021).
- ¹⁸C. Culbertson, “Diffusion coefficient measurements in microfluidic devices,” *Talanta* **56**, 365 (2002).
- ¹⁹D. R. Vogus, V. Mansard, M. V. Rapp, and T. M. Squires, “Measuring concentration fields in microfluidic channels in situ with a Fabry–Perot interferometer,” *Lab Chip* **15**, 1689 (2015).
- ²⁰A. M. Huebner, C. Abell, W. T. S. Huck, C. N. Baroud, and F. Hollfelder, “Monitoring a Reaction at Submillisecond Resolution in Picoliter Volumes,” *Anal. Chem.* **83**, 1462 (2011).
- ²¹A. Yamada, R. Renault, A. Chikina, B. Venzac, I. Pereiro, S. Coscoy, M. Verhulsel, M. C. Parrini, C. Villard, J.-L. Viovy, and S. Descroix, “Transient microfluidic compartmentalization using actionable microfilaments for biochemical assays, cell culture and organs-on-chip,” *Lab Chip* **16**, 4691 (2016).
- ²²M. Hamada and P. de Anna, “A Method to Measure the Diffusion Coefficient in Liquids,” *Transport in Porous Media* (2021), doi:10.1007/s11242-021-01704-0.
- ²³M. A. Unger, H. P. Chou, T. Thorsen, A. Scherer, and S. R. Quake, “Monolithic microfabricated valves and pumps by multilayer soft lithography,” *Science* **288**, 113 (2000).
- ²⁴C. L. Hansen, E. Skordalakes, J. M. Berger, and S. R. Quake, “A robust and scalable microfluidic metering method that allows protein crystal growth by free interface diffusion,” *Proc. Natl. Acad. Sci. USA* **99**, 16531 (2002).
- ²⁵F. Salemme, “A free interface diffusion technique for the crystallization of proteins for X-ray crystallography,” *Arch. Biochem. Biophys.* **151**, 533 (1972).
- ²⁶C. Hansen and S. R. Quake, “Microfluidics in structural biology: smaller, faster em leader better,” *Curr. Opin. Struct. Biol.* **13**, 538 (2003).
- ²⁷B. Derjaguin, S. Dukhin, and M. Koptelova, “Capillary osmosis through porous partitions and properties of boundary layers of solutions,” *J. Colloid Interface Sci.* **38**, 584 (1972).
- ²⁸J. L. Anderson, “Colloid Transport by Interfacial Forces,” *Annu. Rev. Fluid Mech.* **21**, 61 (1989).
- ²⁹S. Marbach and L. Bocquet, “Osmosis, from molecular insights to large-scale applications,” *Chem. Soc. Rev.* **48**, 3102 (2019).
- ³⁰J. Gaube, A. Pfennig, and M. Stumpf, “Vapor-liquid equilibrium in binary and ternary aqueous solutions of poly(ethylene glycol) and dextran,” *J. Chem. Eng. Data* **38**, 163 (1993).
- ³¹“The matlab particle tracking code repository,” <https://site.physics.georgetown.edu/matlab/>.
- ³²J. Goulpeau, D. Troughet, A. Ajdari, and P. Tabeling, “Experimental study and modeling of polydimethylsiloxane peristaltic micropumps,” *J. Appl. Phys.* **98**, 044914 (2005).
- ³³E. Verneuil, A. Buguin, and P. Silberzan, “Permeation-induced flows: consequences for silicone-based microfluidics,” *Europhys. Lett.* **68**, 412 (2004).
- ³⁴G. C. Randall and P. S. Doyle, “Permeation-driven flow in poly(dimethylsiloxane) microfluidic devices,” *Proc. Natl. Acad. Sci. USA* **102**, 10813 (2005).
- ³⁵P. Bacchin, J. Leng, and J.-B. Salmon, “Microfluidic evaporation, pervaporation, and osmosis: From passive pumping to solute concentration,” *Chem. Rev.* **122**, 6938 (2022).
- ³⁶B. Dollet, J.-F. Louf, M. Alonzo, K. Jensen, and P. Marmottant, “Drying of channels by evaporation through a permeable medium,” *J. R. Soc. Interface* **16**, 20180690 (2019).
- ³⁷J.-B. Salmon, L. Soucasse, and F. Doumenc, “Role of solutal free convection on interdiffusion in a horizontal microfluidic channel,” *Phys. Rev. Fluids* **6**, 034501 (2021).
- ³⁸E. Hajizadeh and R. G. Larson, “Stress-gradient-induced polymer migration in Taylor–Couette flow,” *Soft Matter* **13**, 5942 (2017).
- ³⁹J. Xiang, E. Hajizadeh, R. G. Larson, and D. Nelson, “Predictions of polymer migration in a dilute solution between rotating eccentric cylinders,” *J. Rheol.* **65**, 1311 (2021).
- ⁴⁰J. Crank, *The mathematics of diffusion* (Clarendon Press, Oxford, 1975).
- ⁴¹M. Arrio-Dupont, S. Cribier, G. Foucault, P. Devaux, and A. d’Albis, “Diffusion of fluorescently labeled macromolecules in cultured muscle cells,” *Biophys. J.* **70**, 2327 (1996).
- ⁴²D. C. Prieve and R. Roman, “Diffusiophoresis of a rigid sphere through a viscous electrolyte solution,” *J. Chem. Soc., Faraday Trans. 2* **83**, 1287 (1987).
- ⁴³B. Abécassis, C. Cottin-Bizonne, C. Ybert, A. Ajdari, and L. Bocquet, “Boosting migration of large particles by solute contrasts,” *Nat. Mater.* **7**, 785 (2008).
- ⁴⁴R. Nery-Azevedo, A. Banerjee, and T. M. Squires, “Diffusiophoresis in Ionic Surfactant Gradients,” *Langmuir* **33**, 9694 (2017).
- ⁴⁵S. Shin, E. Um, B. Sabass, J. T. Ault, M. Rahimi, P. B. Warren, and H. A. Stone, “Size-dependent control of colloid transport via solute gradients in dead-end channels,” *Proc. Natl. Acad. Sci. USA* **113**, 257 (2016).
- ⁴⁶J. T. Ault, S. Shin, and H. A. Stone, “Diffusiophoresis in narrow channel flows,” *J. Fluid Mech.* **854**, 420 (2018).
- ⁴⁷B. M. Alessio, S. Shim, E. Mintah, A. Gupta, and H. A. Stone, “Diffusiophoresis and diffusioosmosis in tandem: Two-dimensional particle motion in the presence of multiple electrolytes,” *Phys. Rev. Fluids* **6**, 054201 (2021).
- ⁴⁸Y. Gu, V. Hegde, and K. J. Bishop, “Measurement and mitigation of free convection in microfluidic gradient generators,” *Lab Chip* **18**, 3371 (2018).
- ⁴⁹D. Velegol, A. Garg, R. Guha, A. Kar, and M. Kumar, “Origins of concentration gradients for diffusiophoresis,” *Soft Matter* **12**, 4686 (2016).
- ⁵⁰B. Abécassis, C. Cottin-Bizonne, C. Ybert, A. Ajdari, and L. Bocquet, “Osmotic manipulation of particles for microfluidic applications,” *New J. Phys.* **11**, 75022 (2009).
- ⁵¹J. Palacci, B. Abecassis, C. Cottin-Bizonne, C. Ybert, and L. Bocquet, “Colloidal Motility and Pattern Formation under Rectified Diffusiophoresis,” *Phys. Rev. Lett.* **104**, 138302 (2010).
- ⁵²N. Shi, R. Nery-Azevedo, A. I. Abdel-Fattah, and T. M. Squires, “Diffusiophoretic Focusing of Suspended Colloids,” *Phys. Rev. Lett.* **117**, 258001 (2016).
- ⁵³S. Shin, O. Shardt, P. B. Warren, and H. A. Stone, “Membraneless water filtration using CO₂,” *Nat. Commun.* **8**, 15181 (2017).
- ⁵⁴J. S. Paustian, C. D. Angulo, R. Nery-Azevedo, N. Shi, A. I. Abdel-Fattah, and T. M. Squires, “Direct Measurements of Colloidal Solvophoresis under Imposed Solvent and Solute Gradients,” *Langmuir* **31**, 4402 (2015).
- ⁵⁵L. R. Lechlitner and O. Annunziata, “Macromolecule Diffusiophoresis Induced by Concentration Gradients of Aqueous Osmolytes,” *Langmuir* **34**, 9525 (2018).
- ⁵⁶I. Williams, S. Lee, A. Apriceno, R. P. Sear, and G. Battaglia, “Diffusioosmotic and convective flows induced by a nonelectrolyte concentration gradient,” *Proc. Natl. Acad. Sci. USA* **41**, 25263 (2020).
- ⁵⁷P. O. Staffeld and J. A. Quinn, “Diffusion-induced banding of colloid particles via diffusiophoresis. 2. Non-electrolytes,” *J. Colloid Interface Sci.* **130**, 88 (1989).
- ⁵⁸C. Lee, C. Cottin-Bizonne, A. L. Biance, P. Joseph, L. Bocquet, and C. Ybert, “Osmotic flow through fully permeable nanochannels,” *Phys. Rev. Lett.* **112**, 244501 (2014).
- ⁵⁹C. Lee, C. Cottin-Bizonne, R. Fulcrand, L. Joly, and C. Ybert, “Nanoscale Dynamics versus Surface Interactions: What Dictates Osmotic Transport?” *J. Phys. Chem. Lett.* **8**, 478 (2017).
- ⁶⁰R. P. Sear and P. B. Warren, “Diffusiophoresis in nonadsorbing polymer solutions: the Asakura-Oosawa model and stratification in drying films,” *Phys. Rev. E* **96**, 062602 (2017).
- ⁶¹J. Zhou, Y. Jiang, and M. Doi, “Cross Interaction Drives Stratification in Drying Film of Binary Colloidal Mixtures,” *Phys. Rev. Lett.* **118**, 108002 (2017).
- ⁶²M. Schulz, R. W. Smith, R. P. Sear, R. Brinkhuis, and J. L. Keddie, “Diffusiophoresis-Driven Stratification of Polymers in Colloidal Films,” *ACS Macro Lett.* **9**, 1286 (2020).
- ⁶³C. R. Rees-Zimmerman and A. F. Routh, “Stratification in drying films: a diffusion–diffusiophoresis model,” *J. Fluid Mech.* **928**, A15 (2021).

- ⁶⁴M. Schulz, R. Brinkhuis, C. Crean, R. P. Sear, and J. L. Keddie, "Suppression of self-stratification in colloidal mixtures with high Péclet numbers," *Soft Matter* **18**, 2512 (2022).
- ⁶⁵W. R. Young and S. Jones, "Shear dispersion," *Phys. Fluids A* **3**, 1087 (1991).
- ⁶⁶W. B. Russel, D. A. Saville, and W. R. Schowalter, *Colloidal dispersions* (Cambridge University Press, 1989).
- ⁶⁷H. Brenner, "The slow motion of a sphere through a viscous fluid towards a plane surface," *Chem. Eng. Sci.* **16**, 242 (1961).
- ⁶⁸Y. Avni, S. Komura, and D. Andelman, "Brownian motion of a charged colloid in restricted confinement," *Phys. Rev. E* **103**, 042607 (2021).
- ⁶⁹O. Annunziata and A. Fahim, "A unified description of macroion diffusiophoresis, salt osmotic diffusion and collective diffusion coefficient," *Int. J. Heat Mass Transfer* **163**, 120436 (2020).
- ⁷⁰P. Cochard-Marchewka, *Development of a microfluidic device allowing the study of the viscosity of concentrated protein solution, over a wide range of concentration*, Ph.D. thesis, Université PSL (2022).
- ⁷¹C. L. Vestergaard, P. C. Blainey, and H. Flyvbjerg, "Optimal estimation of diffusion coefficients from single-particle trajectories," *Phys. Rev. E* **89**, 022726 (2014).